# DNS of $CO/H_2$/air ignition in a constant volume enclosure relevant to direct injection HCCI engines

**F. Zhang*, J. F. Yu, R. Yu, M. Jangi and X.S. Bai**
Fan.Zhang@energy.lth.se
Division of Fluid Mechanics, Lund University, 22100 Lund, Sweden

## Abstract
Two-dimensional direct numerical simulation (2D-DNS) is used to investigate the reaction zone structures of syngas combustion in a constant volume enclosure relevant to the conditions at the top-dead-center of direct injection homogeneous charge compression ignition (HCCI) engines. The aim is to rectify the effect of turbulence and combustor pressure on the ignition process. The fuel, a mixture of CO and $H_2$ with a 1:1 mass ratio, is initiated in the centre of the domain. The fuel mixes with the surrounding hot air under three different pressure and/or turbulence intensity conditions. The overall ignition delay time, the first ingition sites and the ignition front propagation are simulated. Consistent with previous DNS results, it is noted that auto-ignition is not first started at the stochiometric mixture, but rather in lean mixtures where the local temperature is higher and scalar dissipation rate is low. The first ignition spots with the shortest ignition delay time are found to depend on the turbulence intensity, initial pressure and temperature. With higher turbulence intensity the ignition delay time is longer, and the ignition duration is longer. With higher combustor pressure, the igntion delay time is also longer but the ignition zone is significantly shorter. Compared with the perfectly homogeneous mixture, the igition delay time in the turbulence cases is shorter, owing to differential diffusion and stratifications in composition and temperature.

## Introduction
Homogeneous charge compression ignition (HCCI) engine is a novel concept that makes use of the benefits of spark-ignition engines by using premixed fuel/air mixture and diesel engines that employs compression ignition with high compression ratios. Therefore, HCCI engines offer low soot, $NO_x$ and particle emissions, and high engine efficiency. The most difficult technical problem in a HCCI engine is the control of the initiation of combustion, since the ignition process is very sensitive to the variation of the flow condition. Furthermore, once it is ignited, the homogeneous mixture in the cylinder can ignite almost at the same time [1,2]. Thus, a HCCI engine may suffer from the high pressure-rise rate and high heat release rate.

Several authors have reported the formation of ignition kernels under different turbulence conditions and the subsequent propagation of the reaction zones in HCCI engines. It was found that turbulence could play an important role in the ignition process. The ignition sites are shown to rather randomly distribute in the cylinder in most cases [3,4]. The reaction front can propagate at high speed, typically an order of magnitude faster than turbulent flames. According to Zel'dovich [5] the speed of the reaction front is a function of the ignition delay time (dictated by chemical kinetics) and temperature gradient in the unburned mixture. Gu et al. [6] performed detailed chemical kinetics simulations of stoichiometric $H_2$-CO-air and $H_2$-air mixture in a spherical symmetric configuration. They observed five different modes of reaction front propagation: one is flame propagation and the others are related to auto-ignition. Chen et al. and Hawkes et al. [7,8] performed 2D-DNS to investigate the effect of turbulence and temperature inhomogeneity on HCCI combustion with lean hydrogen air mixture in a constant volume domain. They found that the reaction fronts propagate as both ignition wave

and deflagration wave. The ignition wave is governed by chemical kinetics whereas the deflagration wave is governed by both molecular diffusion and chemical reactions.

From these studies, it is clear that control of HCCI combustion (e.g. pressure-rise rate) may be achieved by optimizing the temperature field. In practice, thermal stratification can be generated naturally in engine cylinders by turbulent heat transfer between the walls and the mixture, or, intentionally by using Exhaust Gas Recirculation (EGR) from the previous cycle. However, using temperature stratification alone may not easily achieve optimal HCCI combustion. An alternative way is using composition stratification to control the heat release rate and thereby pressure-rise rate. The idea is to make use of the difference of the ignition delay time in places with different fuel/air ratio to generate sequential ignition. Yang et al. [9] recently demonstrated experimentally the effect of fuels with single-stage ignition and two-stage ignition on the performance of engines with fuel stratification.

Fuel stratification in HCCI engines can be generated by injecting the fuel directly to the cylinder in the compression stroke, some crank angle degrees before top-dead-center. Before this late injection, a certain amount of fuel is injected to the cylinder at an earlier crank angle (or through port-fuel injection) to form a base mixture with rather homogeneous fuel/air distribution. The injection timing of the second injection is crucial for the fuel stratification in the cylinder, which is the key to achieve successful modulation of the heat release rate. So far, most studies about optimal injection timing are still limited to experiments. It is expected that several parameters would affect the process, for example, turbulence and combustor pressure.

There are a few numerical studies that investigated the effects of turbulence intensity on the mixing and ignition process. Mastorakos et al. [10] first presented autoignition in turbulent shearless mixing layer and studied auto-ignition sites with one-step chemistry incorporating realistic heat release rate. Echekki and Chen [11] studied the most flammable ignition sites using 2D-DNS in a constant volume configuration. Hilbert and Thevenin [12] conducted numerical simulations with detailed chemistry to predict auto-ignition site and ignition time in a 2D turbulent mixing layer. Im et al. [4] preformed 2D-DNS analysis on the auto-ignition of hydrogen and air in a mixing layer. It was indicated that variance of weak turbulence intensity gives rise to small disturbance to ignition delay time but strong turbulence can retard auto-ignition. On the other hand, Hilbert and Thevenin [12] observed that the ignition delay time is always shorter than the laminar ones, and the influence of turbulence Reynolds number is not significant. Doom and Mahes [13] performed 3D DNS to study auto-ignition in turbulent non-premixed $H_2$/Air flame with detailed chemistry. The authors suggested that $T_{MR}$ might be a better indicator in predicting the evolution of auto-ignition.

In the present work, the ignition process of syngas ($CO/H_2$) combustion with hot air in a constant volume enclosure is studied. The aim is to improve the understanding of the ignition process under conditions relevant to direct injection HCCI engines. The first auto-ignition sites are investigated and propagation of the ignition kernels is examined. The effect of turbulence and combustor pressure on the ignition process is investigated.

## Numerical implementation

The reacting flow system considered here is a constant volume enclosure at conditions relevant to HCCI engines with the piston at the top dead center. Yetter et al. [14] $CO/H_2$ chemical kinetic scheme is employed for the present syngas combustion. This mechanism is made up of 12 species $H_2$, H, $O_2$, O, OH, $H_2O$, $HO_2$, $H_2O_2$, CO, $CO_2$, HCO, $N_2$ and 35 steps elementary reactions. The flow speed is low and essentially it can be assumed as low Mach number flow. The physical pressure can be decomposed into two parts, one thermodynamic pressure that is uniform throughout the cylinder and one hydrodynamic pressure that appears in the momentum equation. The mixture considered is in gas phase, without body force, and

with negligible thermal radiation. The governing equations are made up of the transport equations of species mass fraction and energy, the Navier-Stokes equations, and the continuity equation,

$$\rho \frac{DY_k}{Dt} = -\frac{\partial \rho V_{k,i} Y_k}{\partial x_i} + \dot{\omega}_k \tag{1}$$

$$\rho \frac{Du_i}{Dt} = -\frac{\partial p}{\partial x_i} + \tau_{ij} \tag{2}$$

$$\rho C_p \frac{DT}{Dt} = -\sum_{k=1}^{N} h_k \dot{\omega}_k - \left( \rho \sum_{k=1}^{N} C_{p,k} Y_k V_{k,i} \right) \frac{\partial T}{\partial x_i} + \frac{\partial P}{\partial t} + \frac{\partial}{\partial x_i} \left( \lambda \frac{\partial T}{\partial x_i} \right) \tag{3}$$

$$P = \rho R T \sum_{k=1}^{N_{sp}} \frac{Y_k}{W_k} \tag{4}$$

$$\frac{\partial u_i}{\partial x_i} = -\frac{1}{\rho} \frac{D\rho}{Dt} \tag{5}$$

where $\rho$ is density; $Y_k$ is mass fraction of species $k$; $u_i$ is the velocity component in the $x_i$-direction; $V_{k,i}$ is the diffusion velocity of species $k$ in the $x_i$-direction; $\dot{\omega}_k$ is the net formation rate of species $k$; $p$ is the hydrodynamic pressure; $P$ is the thermodynamics pressure; $\tau_{ij}$ is the component of viscous stress tensor; $h_k$ is the specific enthalpy of species $k$; $C_{p,k}$ is the specific heat capacity of species $k$ at constant pressure; $T$ is temperature; $\lambda$ is thermal diffusivity; $W_k$ is the molecular weight of species $k$. $DT/Dt$ denotes the material derivative of temperature.

The continuity equation is written in terms of the material derivative of density, which then makes use of the equation of state (4) to link the continuity equation with the species transport equation (1) and the energy transport equation (3). In this way, robust numerical stability can be achieved when high density gradients exist in the flow field [15].

The fractional step method [15] is used in the numerical solution of the above governing equations. Based on the operator split method the numerical integration of species and energy equations are performed in two steps, first a reacting step where the chemical reaction rates and heat release rates are integrated using a stiffness solver with detailed chemistry, then an advection-diffusion step where the advection and molecular diffusion terms are integrated. In this method most variables can be computed explicitly or semi-explicitly except the hydrodynamic pressure, which is obtained from solution of a variable coefficient Poisson equation derived from the momentum equations and the continuity equation. The pressure equation is solved using a multi-grid method [16,17]. The solver is parallelized based on domain decomposition [18].

The spatial derivatives in the governing equations are discretized using 6$^{th}$ order central difference scheme. The advection term in the species transport and energy transport equations are discretized using a 5$^{th}$ order WENO schemes [19] to avoid wiggles in the species mass fractions that can lead to unphysical solution. The time integration is done using a third order TVD Runge-Kutta scheme. Variable time stepping size is determined by satisfying both advection and diffusion stability limits. More details of numerical methods and solver can be found in [18].

**Initial and boundary conditions**

The computational domain is a square, with a size of 5 mm in each side, within a larger constant volume enclosure. A uniform grid resolution of 2.4 μm mesh size is employed. Periodic conditions are adopted at all boundaries. The initial flow is assumed to be isotropic

turbulent flow satisfying a prescribed turbulent kinetic energy spectrum [20]. In the centre of the square domain, Fig.1a, we place a circular fuel pocket with a radius of 0.87 mm. The initial temperature of the fuel is 300K. The fuel has a CO:H2 ratio of 1:1 on mass basis. Outside the fuel pocket the hot air has a temperature of 1200K. The fuel and air mixes by turbulence forming a stratified charge before ignition. The overall equivalence ratio in the domain is 0.25. This case is similar to Diesel HCCI engine with single fuel injection. Figure 1b shows a zoom-in region of the vorticity contours corresponding to the marked region in Fig.1a. The solid lines correspond to the positive vorticity whereas the dashed lines show negative vorticity. The nearly horizontal lines are the iso-temperature levels. The vorticity field may indicate the size of the turbulence eddies. As seen, the eddies in the cold region are smaller than that in the hot surrounding air, owing to the higher viscosity in the high temperature air zone.

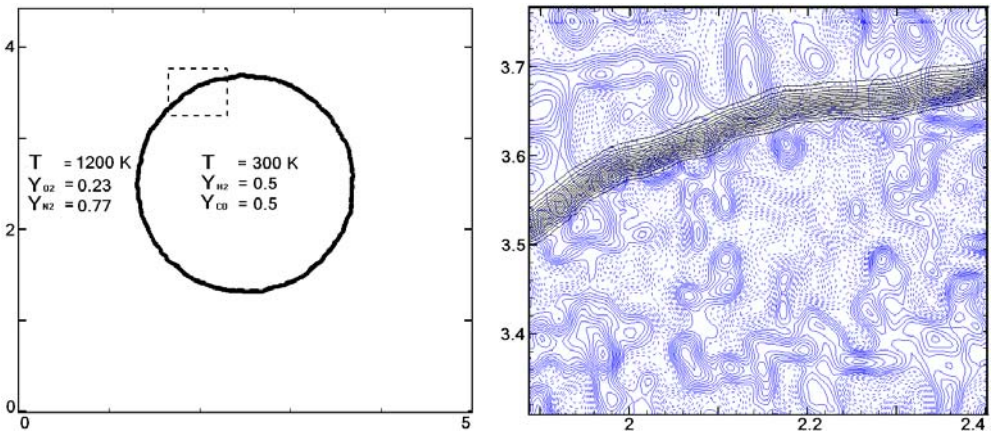


(a) (b)

**Figure 1**. (a) Schematic of the computational domain, (b) zoomed region of the domain with isolines of temperature and vorticity. The unity is millimetre in all figures.

**Table 1.** Initial condition

| Cases | *Re* | *u´* [m/s] | $P_0$ [bar] | *l* [mm] | $\eta$ [mm] | *h* [mm] | grids |
|---|---|---|---|---|---|---|---|
| A | 11.8 | 0.2 | 5 | 1.25 | 0.024 | 0.0024 | 1024×1024 |
| B | 190 | 0.2 | 118 | 1.25 | 0.024 | 0.0024 | 1024×1024 |
| C | 1900 | 2 | 118 | 1.25 | 0.024 | 0.0024 | 1024×1024 |

As shown in Table 1, three cases with the integral velocity (*u´*) of 0.2 m/s and 2 m/s are considered. The Reynolds number (*Re*) based on the integral scale of turbulence varies from 11.8 to 1900. The initial thermodynamic pressure ($P_0$) is 5 bar for Case A and 118 bar for the other cases, representing extremely low load and high load conditions, respectively. The integral length scale (*l*) in all cases is 1.25 mm, whereas the Kolmogorov length scale ($\eta$) is 24 μm. The mesh size (*h*) is 2.4 μm, which is sufficient to resolve the Kolmogorov scales.

**Ignition in homogeneous mixtures**

First, we compute the ignition delay time of the present syngas/air mixtures under constant volume, zero dimensional homogeneous condition. This will serve as a reference data for comparison with the turbulence cases. Figure 2 shows the ignition delay time as a function of mixture fraction. The initial temperature is assumed to be a linear function of the mixture fraction. The mixture fraction (*Z*) is modified according to [21] as:

$$Z = \frac{1/28(Y_H - Y_{H,o})/W_H + (Y_C - Y_{C,o})/W_C - 1/3(Y_O - Y_{O,o})/W_H}{1/28(Y_{H,f} - Y_{H,o})/W_H + (Y_{C,f} - Y_{C,o})/W_C - 1/3(Y_{O,f} - Y_{O,o})/W_H} \quad (6)$$

where $Y_H$, $Y_C$, $Y_O$ are elemental mass fraction; *f* and *o* represent initial condition of fuel and air region. The ignition delay time is defined differently in the literature [11,12], based on either the temperature profile, heat release rate, or species profiles, e.g. H-radicals. Here, the ignition delay time $\tau_0$ is defined as the time with the maximum time derivative of heat release rate.

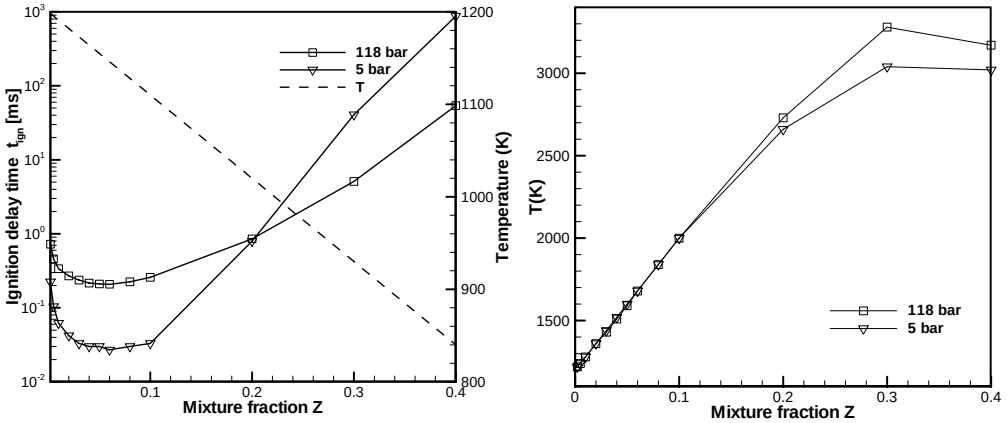


(a) (b)

**Figure 2**. Ignition delay time and initial temperature (a) and adiabatic flame temperature (b) of homogeneous $CO/H_2$/air mixtures in a constant volume enclosure at initial pressure of 5 bar and 118 bar. The results are from numerical calculation using Yetter et al. mechanism [14]. The initial temperature is assumed to be a linear function of mixture fraction.

Shown in Fig. 2a is the auto-ignition delay time of the syngas/air mixture with various initial mixture fraction and temperature. The initial pressures are 5 bar and 118 bar, and the initial temperature ranges from 840 K to 1200 K, which is consistent with the initial conditions of the present DNS cases described in Table 1. Consistent with Ref. [22], Fig. 2a shows that the most reactive mixture fraction $Z_{MR}$=0.06 is leaner than the stoichiometric mixture fraction ($Z_{st}$=0.18). This is owing to the higher initial temperature in the lean mixture. At $Z_{MR}$ the ignition delay time is at its minimum, which is about 0.208 ms for the 118 bar case and 0.027 ms for the 5 bar case. The difference in ignition delay time is attributed to the dependence of chemical kinetic rates on pressure. One pair of important competing reactions under lean fuel conditions are $H + O_2 + M = HO_2 + M$ and $H + O_2 = O + OH$. The former consumes H-radicals while forming $HO_2$ that is relatively less reactive than H-radicals; the latter consumes H-radicals while forming O and OH-radicals that are very reactive. At high pressures, the former is enhanced whereas the latter is suppressed, leading to a less reactive system and thereby longer ignition delay time at high pressures. For very rich mixtures, e.g. $Z > 0.3$, the level of $O_2$ is lower, and the importance of these two reactions are lower, and as such the ignition delay time of the high pressure case is shorter than the low pressure case, owing to higher combustion temperature in the constant volume enclosure.

**Ignition process in case A: low combustor pressure**

Figure 3a shows the time history of the total heat release rate of the homogeneous ignition case at initial pressure of 5 bar, initial temperature of 1146 K, and mixture fraction of 0.06. This case corresponds to the most reactive condition in Fig.2a. In this case ignition starts at 0.02 ms and lasts for about 0.03 ms. Figure 3b shows the time history of the total heat release rate in the domain for case A. In this case ignition starts at 0.0145 ms. The peak heat release rate is around 0.02 ms, and the peak heat release rate is significantly lower than the

corresponding homogeneous case. The ignition delay time is 0.015 ms, which is lower than that of the homogeneous case discussed earlier (0.027 ms for the 5 bar homogeneous mixture), owing to the effect of turbulence.

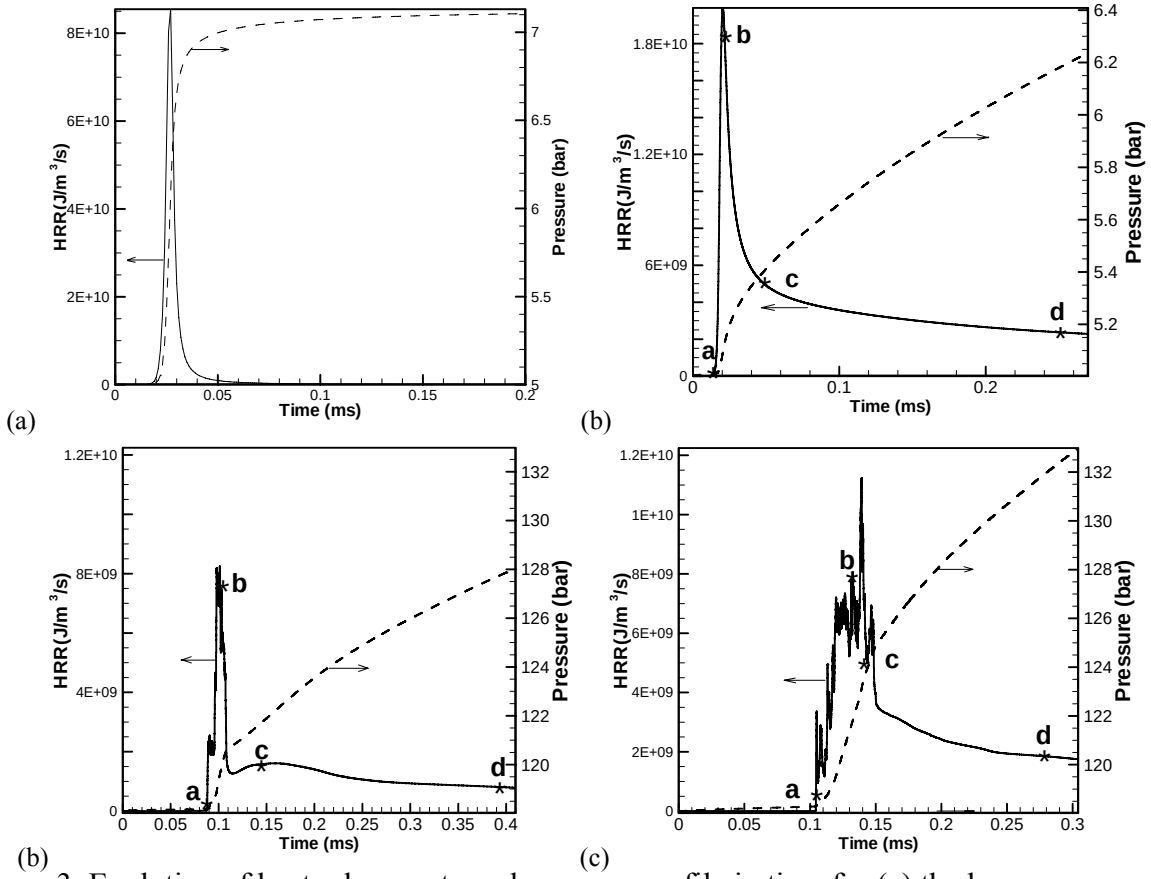


Figure 3. Evolution of heat release rate and pressure profile in time for (a) the homogeneous ignition case, (b) case A, (c) case B, (d) Case C.

To look into details about the ignition process, Figure 4 ($A_a$-$A_d$) show the spatial distribution of heat release rate in the computational domain at four instances of time, corresponding to the instances marked in Fig.3b as points a, b, c and d, respectively. The first ignition sites, shown in Fig.4$A_a$, appear at 0.0145 ms and on the air rich side of the $Z_{MR}$=0.06 line (the dashed line in the figure), which is the most reactive mixture fraction of the homogeneous case discussed earlier. In the air rich side the temperature of the mixture is higher and as such the onset of ignition is earlier. This will be shown further below.

At 0.0207 ms shown in Fig.4$A_b$, the ignition sites are seen in a relatively wide annular region around the most reactive mixture fraction, $Z_{MR}$=0.06, and leaner than the stoichiometric mixture fraction $Z_{st}$=0.18 (shown as the solid lines). The heat release rate is nearly uniform in the reaction zone and it is almost at its highest level (Figs.3b & 4$A_b$). Later on, the heat release rate decreases drastically. At 0.048 ms shown in Fig.4$A_c$, heat release is seen in regions richer than the stoichiometric mixture fraction and leaner than the most reactive mixture fraction. In between these regions the heat release rate is low due to local completion of the fuel consumption. At 0.245 ms shown in Fig.4$A_d$, heat release is seen in the narrow region leaner than the most reactive mixture fraction. As will be demonstrated later, the peak heat release rate between points a and c shown in Fig.3b corresponds to auto-ignition of the stratified fuel/air mixture; after point c, the reaction is controlled by the mixing of fuel and the surrounding air. It is seen that the iso-contours of $Z_{MR}$ and $Z_{st}$ increases in size with time, following the mixing process of the fuel pocket with the surrounding air.

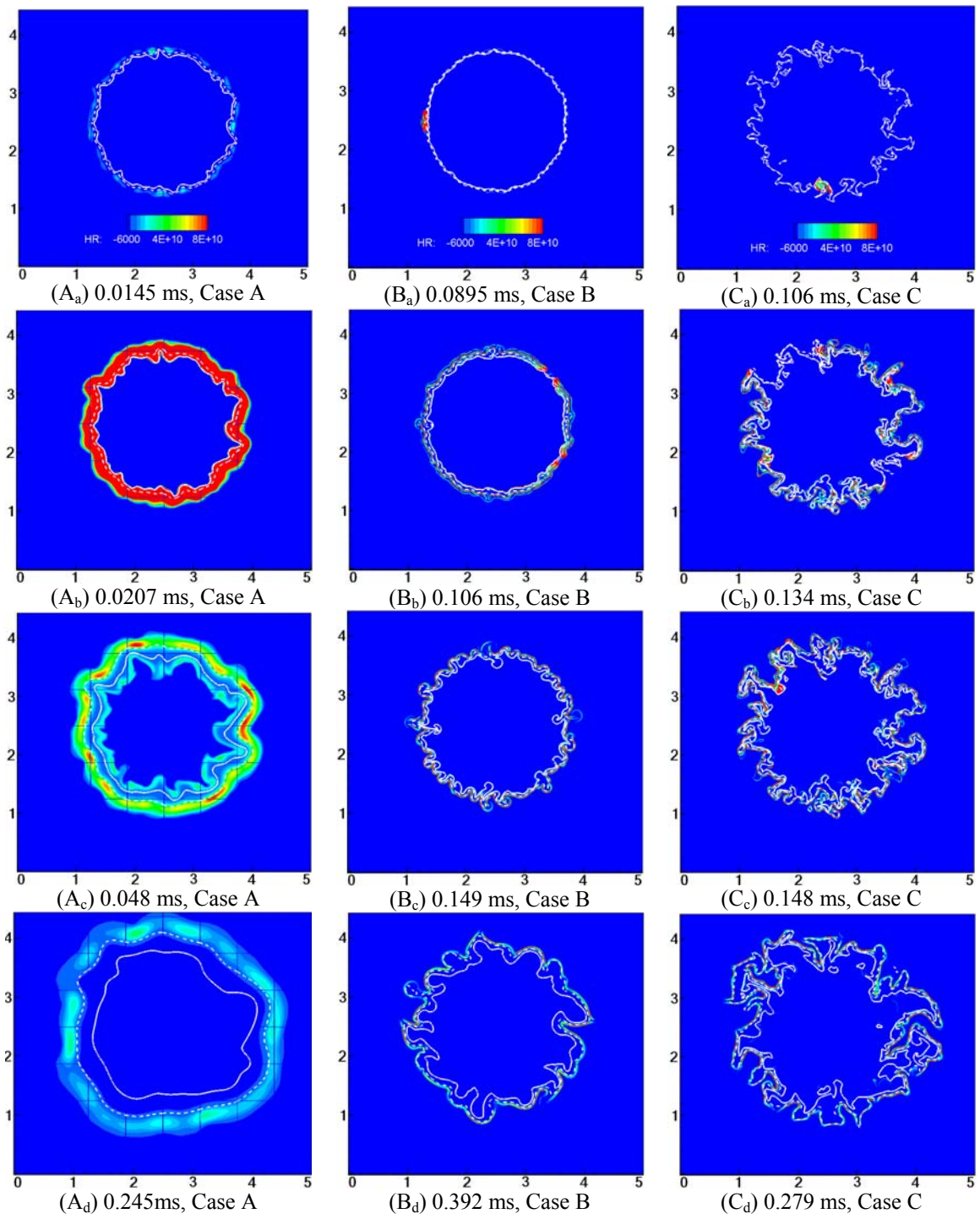


($A_a$) 0.0145 ms, Case A ($B_a$) 0.0895 ms, Case B ($C_a$) 0.106 ms, Case C

($A_b$) 0.0207 ms, Case A ($B_b$) 0.106 ms, Case B ($C_b$) 0.134 ms, Case C

($A_c$) 0.048 ms, Case A ($B_c$) 0.149 ms, Case B ($C_c$) 0.148 ms, Case C

($A_d$) 0.245ms, Case A ($B_d$) 0.392 ms, Case B ($C_d$) 0.279 ms, Case C

Figure 4. Contours of heat release rate at different times during auto-ignition for case A ($A_a$-$A_d$), case B ($B_a$-$B_d$), and case C ($C_a$-$C_d$). Dashed lines denote the most reactive mixture fraction ($Z_{MR}$=0.06) and solid lines denote stoichiometric mixture fraction $Z_{st}$ = 0.18.

**Ignition process in case B: effect of elevated combustor pressure**

Case B differs from case A in the combustor pressure. In case B, the initial pressure is more than 20 times larger than the initial pressure of case A. As a result, the diffusion coefficients of mass and heat in case B are lower than those in case A, resulting in a higher Reynolds number and lower Kolmogorov scale. Figure 3c shows the time history of heat release rate in case B. As seen, the ignition delay time (0.0895 ms) is much longer than that of case A (0.027 ms), however, it is significantly lower than the corresponding homogeneous case with the

most reactive mixture discussed earlier (0.208 ms). This result is consistent with the result of Hilbert and Thevenin [12]. The overall peak rate of heat release in case B is smaller than that in case A. Compared to case A, the longer ignition delay time is largely an effect of pressure on the chemical kinetics as discussed earlier. Compared to the corresponding homogeneous case, the shorter ignition delay time is a result of temperature and composition stratification.

To further examine this phenomenon, distributions of heat release rate at four instances of time (marked as points a-d Fig.3c) are shown in Figs.4 ($B_a$-$B_d$). Compared to the homogeneous case, the first ignition site (Fig.4$B_a$) is on the fuel lean side of $Z_{MR}$ where the local temperature is higher than the corresponding homogeneous case, and this results in earlier onset of the ignition. This is consistent with case A and earlier DNS results. Comparing case B and case A, one can see that the heat release zone in case B is much thinner than that in case A, which is due to the smaller Kolmogorov scale that the molecular mixing is at smaller scales, and the wrinkling scale of the iso-contours of mixture fraction is smaller. The first ignition site appears at small eddies whose size decreases as the combustor pressure increases. This will be further discussed below.

**Ignition process in case C: effect of elevated turbulence**

Case C has higher turbulence intensity and higher Reynolds number than case B. The initial pressures in the two cases are identical. Increasing the intensity of turbulence leads to higher mixing rate and smaller Kolmogorov scale. As such, the growth of the $Z_{st}$ and $Z_{MR}$ lines is faster, and the wrinkling of these lines is more intensive. The ignition delay time is longer, owing to stronger interaction between the ignition process and the heat and mass transfer process. This is consistent with the observation in spark-ignition process and the auto-ignition DNS results of Im et al. [4]. It is likely attributed to the high scalar dissipation rate at the high intensity turbulence conditions, which tends to remove the heat and radicals generated in the ignition site, thereby delaying the ignition process. With higher turbulence intensity in case C, the ignition duration (between point a and c in Fig.3d) is also longer than the corresponding one in case B, owing to larger stratification in the temperature and composition fields. In both case B and case C the heat release zone is seen in very narrow region as compared to the low-pressure case, owing to the smaller scales existing in the field, Fig.4 ($C_a$-$C_d$).

**The first ignition sites**

To understand the effect of turbulence and pressure on the ignition delay time, it is helpful to examine the first ignition sites. The results presented above and previous DNS study on the ignition process of non-premixed fuel/air mixture have shown that the first ignition sites locate in mixtures leaner than the stoichiometric mixtures. This is due to the fact that mixing of cold fuel with hot air results in a certain correlation between the temperature of the mixture and the fuel/air ratio in the mixture. Leaner mixture has higher temperature and therefore the most ignitable mixture is often in the lean mixtures with higher temperature. This phenomenon has been observed by several authors, as reviewed by Mastorakos [22]. Furthermore, previous studies have shown that under weak turbulence intensity conditions, the ignition delay time is not sensitive to turbulence; under high intensity turbulence conditions, however, turbulence has a mixed effect. Im et al. [4] reported that increasing turbulence retarded the ignition process, whereas Hilbert and Thevenin [12] found a rather insignificant dependence of ignition delay time on turbulence Reynolds number. The present results appear to be consistent with that of Im et al. [4]. However, it should be kept in mind that the studied flow conditions and fuel are different; thus, care must be taken before comparing these results.

Figure 5 shows the distribution of $HO_2$ and heat release rate and the instantaneous flow tracelines in a zoomed region at the instance of time of first ignition sites for case A and case

C. The iso-lines of temperature and mixture fraction are also shown in the figure. It appears that the iso-lines of temperature and mixture are nearly 'parallel', due to the similarity of the mixing process and the heat transfer process. At the first ignition sites, however, the iso-lines and temperature and mixture fraction are not 'parallel'; along the iso-line of mixture fraction, the temperature at the first ignition site is higher than that in other places. The ignition spots are of the size of the vorticity core, but not inside the vortex core. Contrary to this, some authors have observed that the first ignition sites locate inside the vorticity core [22]. It should be pointed out that ignition process has a strong history effect; during the induction process the vortices move and the intermediate products formed in the induction process may not follow the movement of vortices.

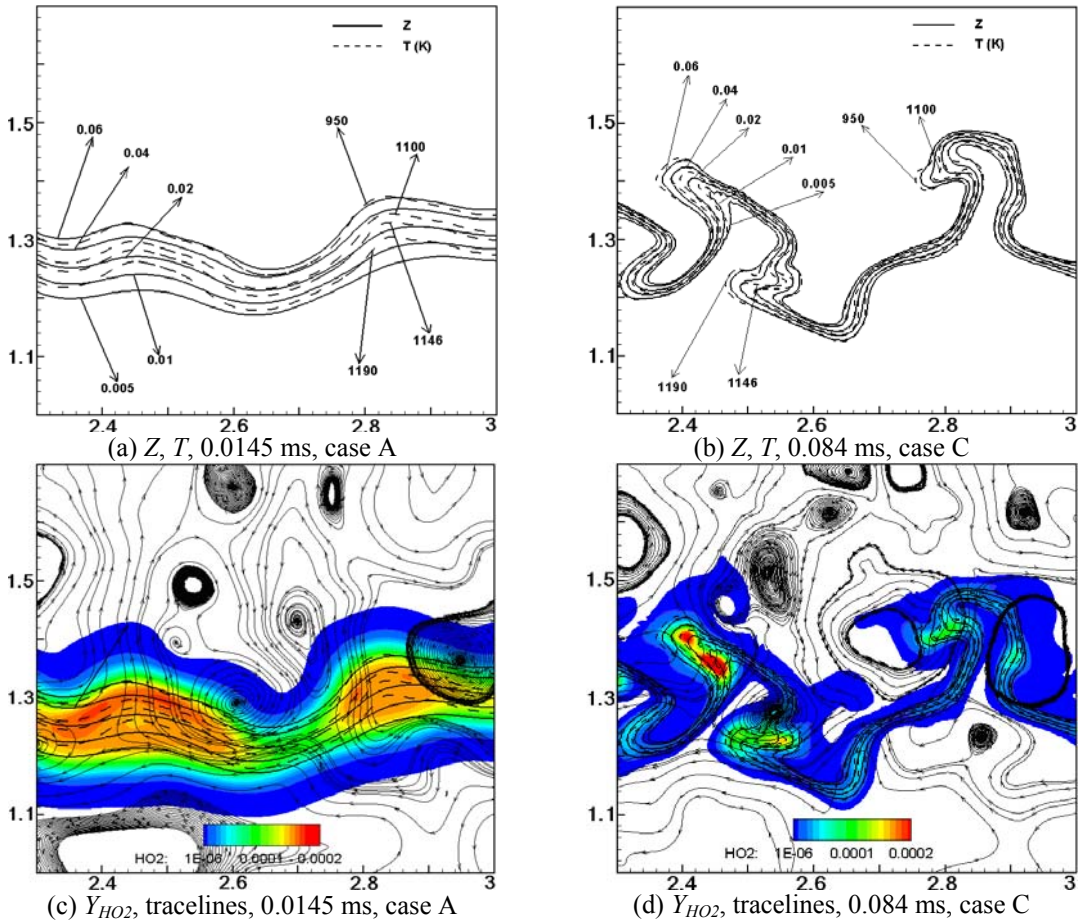


(a) $Z$, $T$, 0.0145 ms, case A (b) $Z$, $T$, 0.084 ms, case C

(c) $Y_{HO2}$, tracelines, 0.0145 ms, case A (d) $Y_{HO2}$, tracelines, 0.084 ms, case C

Figure 5. Iso-lines of temperature and mixture fraction, tracelines, and distribution of $HO_2$ mass fraction at the instance of time for the first ignition sites.

Figure 6 shows a scatter plot of temperature as a function of mixture fraction at the instance of first ignition and at the later instances of time for cases B and C. It is seen that at the instance of first ignition, Fig.6a (case B) and Fig.6d (case C), the ignition sites are at the mixture with mixture fraction ranging from $0.005 < Z < 0.1$; the highest temperature after the ignition is at the mixture fraction around 0.04, which is leaner than $Z_{MR} = 0.06$. The temperature of unburned mixture (the low branch in the figure) in the lean mixture ($Z < 0.02$) is rather close to the temperature of hot air (1200 K), which is the reason that these ultra lean mixtures are among the first ignited ones. At later instances of time, e.g. Fig. 6b and 6e, ignition occurs in rather wider range of mixture fraction (evident in the scatter of temperature and the less dense distribution of cells in the lower branch of the figures). At even later instances of time, Fig.6c and 6f, the entire low branch has disappeared, indicating the end of

the ignition process. For mixture with Z > 0.4, the temperature is still low, which corresponds to the unburned fuel zone partially mixed with hot combustion products. The fuel will subsequently mix with the air outside the fuel zone and burns out in a diffusion flame mode, corresponding to the lower heat release rate in Fig. 3 between points c and d.

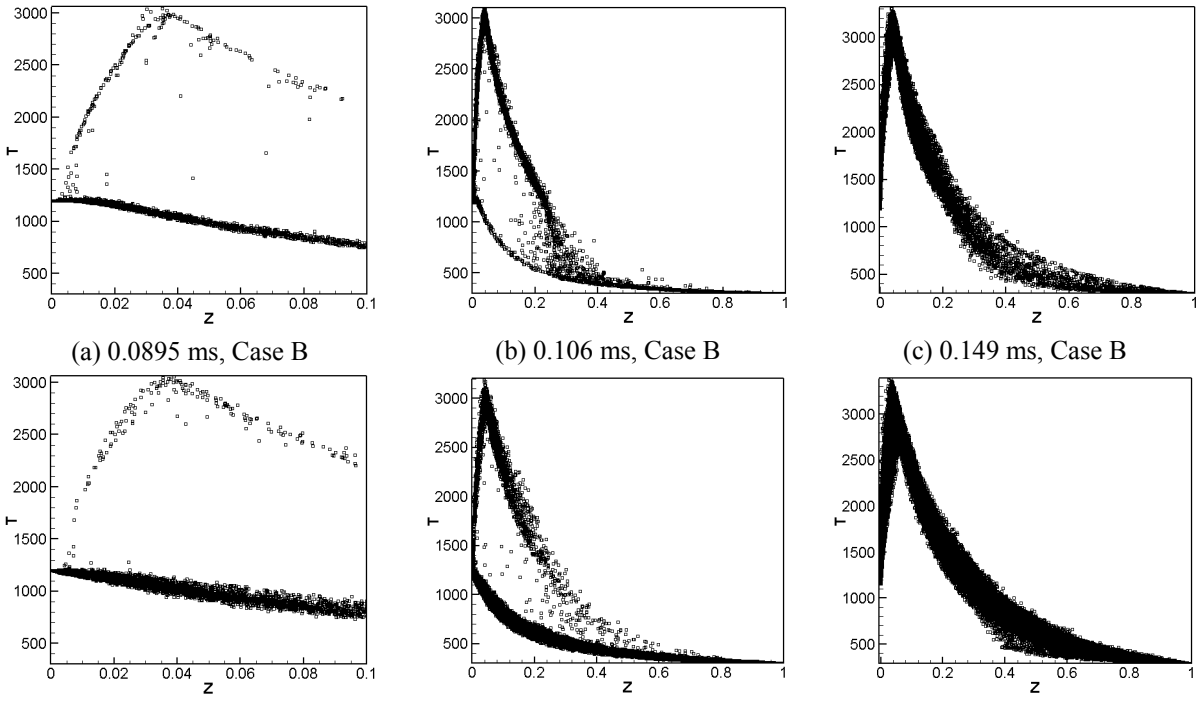


(a) 0.0895 ms, Case B (b) 0.106 ms, Case B (c) 0.149 ms, Case B

(d) 0.106 ms, Case C (e) 0.117 ms, Case C (f) 0.279 ms, Case C

Figure 6. Scatter plots of the temperature in the mixture fraction space for case B (a-c) and case C (d-f).

**Effect of scalar dissipation rate**

Previous DNS studies have reported the importance of scalar dissipation rate in the ignition process. Ignitions were shown to occur first at locations with the most reactive mixture and low local scalar dissipation rate. To examine this, Figure 7 shows the distribution of CO mass fraction (a, b) and OH mass fraction (c, d) for case A and case C, at the instances that first ignition sites appear. The figure also shows iso-lines of mixture fraction, temperature around the first ignition sites, and scalar dissipation rate defined based on the mixture fraction field. It is seen that on the fuel rich side and air rich side the scalar dissipation rate is low. Around the stoichiometric mixtures the scalar dissipation rate is higher. Along the iso-line of $Z_{MR}$=0.06, the scalar dissipation rate for case A is about 1 $s^{-1}$, whereas at the first ignition sites the scalar dissipation rate is between 0.01 $s^{-1}$ and 0.1 $s^{-1}$. It appears that the first ignition sites (0.005<Z<0.02) occur at mixtures leaner than $Z_{MR}$, not only due to the locally higher temperatures (as shown earlier in Fig.5) but also owing to the lower local scalar dissipation rate in the leaner mixtures. For the higher pressure and high turbulence intensity case (case C) similar observations can be made.

**Summary**

In this paper we report on numerical simulations of the effect of turbulence and combustor pressure on auto-ignition of H2/CO/air mixtures under pressure and temperature conditions relevant to direct injection diesel engines. The numerical simulations are carried out in a 2D square domain in a large constant volume enclosure. The simulations are based on the CO/H2 mechanism of Yetter et al. and detailed transport properties. The results show that the ignition

delay time of turbulent cases is considerably shorter than the corresponding homogeneous mixtures. This is due to the onset of the first ignition sites at mixtures leaner and temperatures higher than the most reaction mixtures in the homogeneous mixtures. The most reactive sites are not in the stoichiometric mixtures due to the fact that in direct injection conditions, the stoichiometric mixtures at often at high local scalar dissipation rate conditions, in addition to the relatively lower local temperature. It is found that higher turbulence can smooth the peak heat release rate and increase ignition delay time. Higher combustor pressure leads to longer ignition time and thinner ignition zone, owing to the decrease of the Kolmogorov length scales.

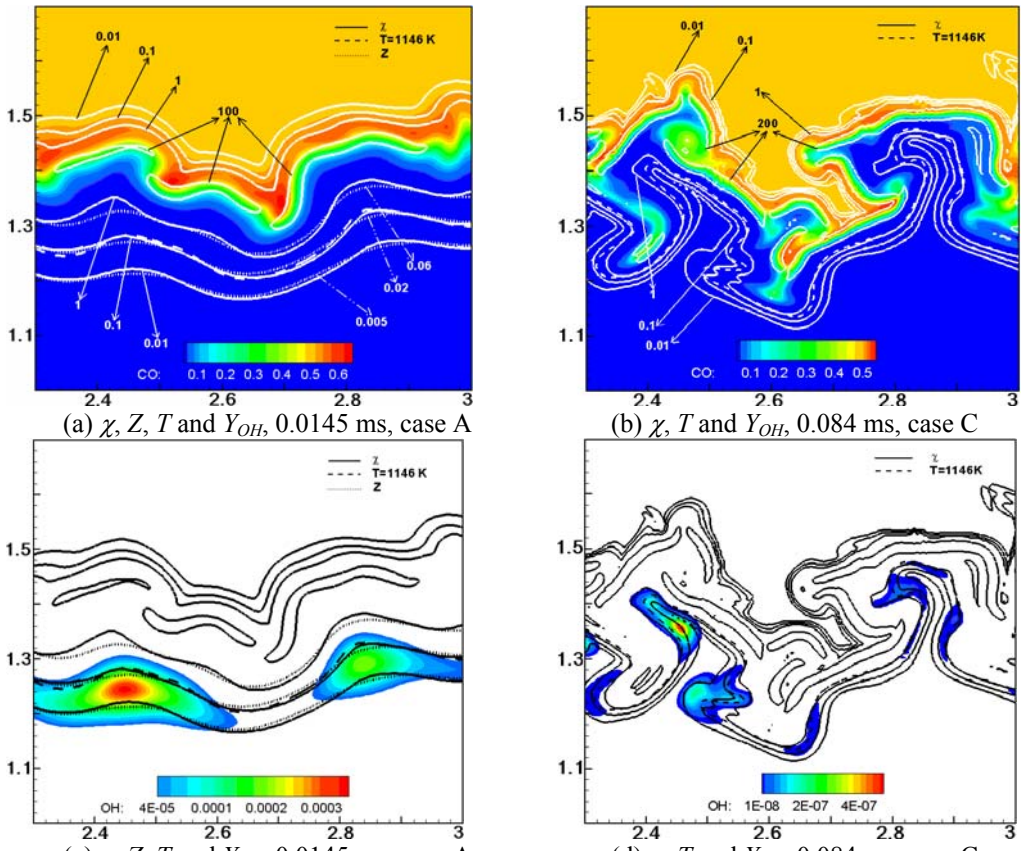


(a) $\chi$, $Z$, $T$ and $Y_{OH}$, 0.0145 ms, case A

(b) $\chi$, $T$ and $Y_{OH}$, 0.084 ms, case C

(c) $\chi$, $Z$, $T$ and $Y_{OH}$, 0.0145 ms, case A

(d) $\chi$, $T$ and $Y_{OH}$, 0.084 ms, case C

Figure 7. Snapshots of $Y_{OH}$ and $Y_{CO}$ mass fractions at time $t$ = 0.0145 ms for case A and 0.084 ms for case C. Also shown in the figure are iso-lines of mixture fraction, temperature and scalar dissipation rate.

**Acknowledgements**

This work was sponsored by the Swedish Research Council (VR), the Competence Centre for Combustion Process at Lund University (KC-FP), and the national Centre for Combustion Science and Technology (CeCOST). F. Zhang and J.F. Yu were sponsored by China Scholarship Council (CSC).

**References**

[1] Christensen, M., "*HCCI Combustion-Engine Operation and Emission Characteristics*", PH.D thesis, Lund Institute of Technology, 2002.

[2] F. Zhao, T.A., D. Assanis, J. Dec, J. Eng, P. Najt, "Homogeneous Charge Compression Ignition (HCCI) Engines, Key Research and Development Issues", *Society of Automotive Engineers*, 2002: p. 14.

[3] Seyfried, H., Olofesson, J., Sjöholm, J., Richter, M., Alden, M., Hultqvist, A., Johansson, B., "High-Speed PLIF Imaging for Investigation of Turbulence Effects on Heat Release Rates in HCCI Combustion", *SAE technical paper*, 2007. **2007-01-0213**.
[4] Im, H.G., Chen, J. H., Law, C. K., "Ignition of hydrogen-air mixing layer in turbulent flows", *Twenty-Seventh Symposium (International) on Combustion, Vols 1 and 2*, 1998: p. 1047-1056 3274.
[5] Zeldovich, Y.B., "Regime Classification of an Exothermic Reaction with Nonuniform Initial Conditions", *Combustion and Flames.* 1980. 39: p. 211-214.
[6] Gu, X.J., Emerson, D.R., Bradley, D., "Modes of reaction front propagation from hot spots", *Combustion and Flame*. 2003. 133(1-2): p. 63-74.
[7] Chen, J.H., Hawkes, E. R., Sankaran, R., Mason, S. D., Im, H. G., "Direct numerical simulation of ignition front propagation in a constant volume with temperature inhomogeneities - I. Fundamental analysis and diagnostics", *Combustion and Flame*. 2006. **145**(1-2): p. 128-144.
[8] Hawkes, E.R., Sankaran, R., Pebay, P. P., Chen, J. H., "Direct numerical simulation of ignition front propagation in a constant volume with temperature inhomogeneities - II. Parametric study", *Combustion and Flame*. 2006. **145**(1-2): p. 145-159.
[9] Yang, Y., Dec, J. E., Dronniou, N., Sjoberg, M., "Tailoring HCCI heat-release rates with partial fuel stratification: Comparison of two-stage and single-stage-ignition fuels", *Proceedings of the Combustion Institute*, 2011. **33**: p. 3047-3055.
[10] Mastorakos, E., Baritaud, T. A., Poinsot, T. J., "Numerical simulations of autoignition in turbulent mixing flows", *Combustion and Flame.* 1997. **109**(1-2): p. 198-223.
[11] Echekki, T., Chen, J. H., "Direct numerical simulation of autoignition in non-homogeneous hydrogen-air mixtures", *Combustion and Flame.* 2003. **134**(3): p. 169-191.
[12] Hilbert, R., Thevenin, D., "Autoignition of turbulent non-premixed flames investigated using direct numerical simulations", *Combustion and Flame.* 2002. **128**(1-2): p. 22-37.
[13] Doom, J., Mahesh, K. , "DNS of auto-ignition in turbulent diffusion $H_2$/air flames", 47th *AIAA Aerospace Sciences Meeting Including The New Horizons Forum and Aerospace Exposition*, 2009. **240**.
[14] Yetter, R.A., Dryer, F. L., Rabitz, H., "A Comprehensive Reaction-Mechanism for Carbon-Monoxide Hydrogen Oxygen Kinetics", *Combustion Science and Technology*. 1991. **79**(1-3): p. 97-128.
[15] Day, M.S. and J.B. Bell, "Numerical simulation of laminar reacting flows with complex chemistry", *Combustion Theory and Modelling*. 2000. **4**(4): p. 535-556.
[16] Bai, X.S., Fuchs, L., "Modeling of turbulent reacting flows past a bluff body: assessment of accuracy and efficiency", *Computers Fluids*. 1994. **23**: p. 507-521.
[17] Gullbrand, J., Bai, X.S., Fuchs, L., "High-order Cartesian grid method for calculation of incompressible turbulent flows", Int. J. Numer. *Meth. Fluids.* 36:687-709, 2001.
[18] Yu, R., "*Large Eddy Simulation of Turbulent Flow and Combustion in HCCI engines*", PH.D thesis, Lund Institute of Technology, 2008.
[19] Jiang, G.S., Shu, C. W., "Efficient implementation of weighted ENO schemes", *Journal of Computational Physics.* 1996. **126**(1): p. 202-228.
[20] Pope, S.B., *Turbulent Flows.* (Cambridge University Press, Cambridge, UK, 2000), 2000.
[21] Bilger, R.w., Starner, S.H., Kee, R.J., "On reduced mechanisms for methane-air combustion in nonpremixed flames", *Combustion and Flame.* 1990.80(2):p. 135-149.
[22] Mastorakos, E., "Ignition of turbulent non-premixed flames", *Progress in Energy and Combustion Science*, 2009. **35**(1): p. 57-97.